JOURNAL OF SPACECRAFT AND ROCKETS
Vol. 31, No. 5, September–October 1994

Multibody-Plasma Interactions: Charging in the Wake

J. Wang,* P. Leung,* H. Garrett,* and G. Murphy*
Jet Propulsion Laboratory, California Institute of Technology, Pasadena, California 91109

Multibody-plasma interactions occur when two or more charged bodies simultaneously interact with the surrounding plasma as well as each other. This paper concerns a basic type of such interactions in the ionosphere: the charging of a free flyer in the wake of a large plate structure. Computer particle simulations are coupled with charging calculations to obtain the free-flyer charging potentials in the wake of a plate, which can be either floating or biased. The conditions under which multibody interaction occurs are identified. It is shown that a severe charging zone exists in the near wake of a large floating plate under the nightside auroral-electron condition. Whether the plate structure is biased or floating, a large potential difference always exists between the plate and a free flyer docking in the wake. The effects of this wake charging on spacecraft docking operations are discussed.

Nomenclature

C_s = ion sound speed
d_{sh} = sheath thickness
e = electron charge
J_i, J_e, J_{ea} = current density: ambient ion, ambient electron, and auroral electron, respectively
J_{si}, J_{se} = current density: secondary electron due to incident ion and electron, respectively
J_{bse}, J_{ph} = current density: backscattered electron and photoelectron, respectively
K = Boltzmann constant
L_p = plate length
M_0 = ambient-ion-flow Mach number
m_e, m_i = electron and ion mass, respectively
n_i, n_e, n_{ea} = ambient ion, electron, and auroral electron density, respectively
n_0, n_{ea0} = unperturbed ambient plasma and auroral electron density, respectively
R = half plate length
R_{ci} = ion Lamor radius
T_i, T_e, T_{ea} = ambient ion, electron, and auroral electron temperature, respectively
V_0, v_{ti}, v_{te} = orbital, ion thermal, and electron thermal velocity, respectively
x_p, y_p = location of the plate center
x_w, y_w = location of the free-flyer center
ζ = ratio of sheath thickness to plate dimension
λ_d = Debye length
Φ = electric potential
Φ_p, Φ_w = potential of the plate and of the free flyer

I. Introduction

FUTURE space missions in the ionosphere will increasingly involve multibody-plasma interactions (MPI). Such interactions occur when two or more charged bodies immersed in a plasma simultaneously interact with the plasma and each other. Examples of space operations involving MPI include docking of two spacecraft, robotics servicing, astronauts on extravehicular activities (EVA), etc. The upcoming Charged Hazards and Wake Studies (CHAWS) experiment aboard the Wake-Shield Facility also provides an example of MPI. It has been realized that MPI may have adverse effects on spacecraft operation and, in certain situations, represent a significant safety hazard.[1,2]

An MPI issue that is particularly important to space-system reliability and operations in the ionosphere is the wake charging problem. A spacecraft in the ionosphere has an orbital velocity $V_0 \simeq 8$ km/s. Since $v_{ti} \ll V_0 \ll v_{te}$ (where v_{ti} and v_{te} are the ion and electron thermal velocity respectively), the spacecraft creates behind it a plasma wake within which the ion current is reduced to a fraction of the ambient level. If a suitable energetic electron environment is present, such as the polar auroral electron environment, a small free flyer or an astronaut in the wake could easily be charged to a dangerously high voltage on account of the lack of ion current. Furthermore, for spacecraft docking operations, wake charging may lead to significantly different voltages between the docking surfaces, and thus trigger electrostatic discharges (ESD).

In this paper, we study the wake charging problem for an orbiting system in the auroral zone. The auroral zone, the region between roughly 60 and 70 deg geomagnetic latitude, is crossed four times per pass for a polar orbit. Within this region, the flux of electrons from hundreds of electron volts to a few tens of keV regularly reaches[3,4] 1 to 10 nA/cm^2. Gussenhoven et al. studied DMSP satellite charging data and found that the hot auroral electrons can lead to kilovolt-level negative charging.[3]

Several studies have discussed issues related to the wake charging problem.[5–9] For instance, Katz et al. used orbit-limited theory to estimate the ion-current collection by a small object in the Space Shuttle wake and obtained an upper bound on the wake charging potential.[5] Enloe et al. studied the current-voltage characteristics for a probe in the wake using laboratory simulations.[9] However, no studies have attempted a self-consistent calculation of wake charging, taking into account the complex coupling between the plasma wake and the free flyer's sheath. The plasma wake itself has been a subject of many laboratory experiments,[10–14] theoretical studies,[15–18] and in situ measurements.[19–21] Recently, Wang and Hastings studied in detail the formation and structure of the plasma wake behind large space platforms, using computer particle simulations.[18] The wake model developed in Ref. 18 is extended for this current study of wake charging.

We consider a two-body system orbiting in the ionosphere as illustrated in Fig. 1. This generic two-body system consists of a large plate and a small free flyer in its wake. The essence of this problem is to solve self-consistently for the electric field generated by these two charged bodies, the plasma motion in this electric field, and the charging potential and the current collection of the free flyer. In this paper, such a self-consistent solution is obtained by using computer particle simulations coupled with charging calculations. The formulation and approach are described in Sec. II. In Sec. III, we study charging in the wake of a plate with a floating potential. The interaction between a biased plate and a free flyer is discussed in Sec. IV. For both cases, the free flyer's charging level is studied as a function of its location in the wake, and the conditions for MPI to occur are discussed. Section V contains a summary and conclusions.

Received April 28, 1993; revision received Feb. 22, 1994; accepted for publication Feb. 23, 1994.

*Member Technical Staff, MS301-460, 4800 Oak Grove Drive. Member AIAA.

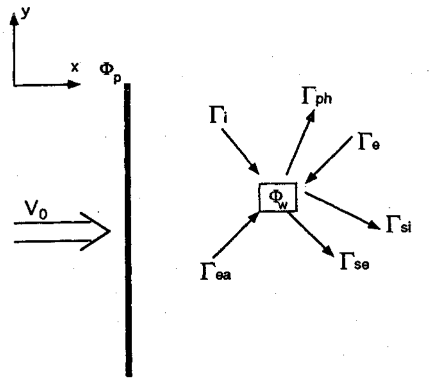

Fig. 1 Illustration of the two-body system in the moving reference frame fixed with the system. The fluxes of ambient plasma (Γ_i, Γ_e), auroral electrons (Γ_{ea}), secondary electrons (Γ_{si}, Γ_{se}), and photoelectrons (Γ_{ph}) received by the free flyer are also indicated.

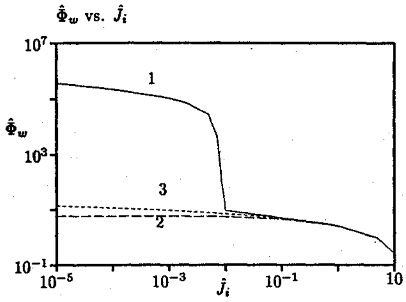

Fig. 2 Equilibrium charging potential of an isolated body, $\hat{\Phi}_w$, as a function of $\hat{J}_i$. Curve 1: nightside, auroral-electron condition; curve 2: dayside, auroral-electron condition; curve 3: nightside, no-auroral-electron condition.

II. Formulation and Approach

We consider a plasma environment typical for a 300-km polar orbit. The plasma is a mainly O^+ "cold" plasma (density n_0 and temperatures T_e, T_i) when there are no auroral electrons. Typical values of the density and temperature of the cold plasma are $n_0 \simeq 2 \times 10^5$ cm^{-3}, $T_e \simeq 0.1$ eV, and $T_i \simeq 0.5 T_e$. Under the auroral electron condition, a "hot" auroral electron population is also present. Typically the auroral electrons has a density $n_{ea0} \simeq 1$ cm^{-3} and a temperature[3] $T_{ea} \simeq 5$ keV. These parameters will be used throughout this paper.

For convenience of the analysis, we normalize the spatial dimension by the Debye length ($\lambda_D = \sqrt{KT_e/4\pi n_0 e^2}$) as $\hat{X} = X/\lambda_D$, and the potential by the ambient electron temperature T_e as $\hat{\Phi} = e\Phi/KT_e$. The current density is normalized by the Bohm current density en_0C_s as $\hat{J}_i = J_i/en_0C_s$, where $C_s = \sqrt{KT_e/m_i}$ is the ion acoustic velocity. For the ambient environment considered here, $C_s \simeq 1$ km/s and the Bohm current density is about $en_0C_s \simeq 3.2 \times 10^{-5}$ A/m^2. Using this normalization, the streaming ambient ions have a current density $\hat{J}_{i0} \simeq 8$ ($M_0 = V_0/C_s \simeq 8$). In the rest of this paper, λ_D, T_e, and en_0C_s will be used as the units for the length, potential, and current density, respectively, whenever no units are stated.

Charging Calculation

The equilibrium charging state for a uniformly conducting body is determined by the total-current balance condition $\sum I(\Phi_w) = 0$, where Φ_w is the body potential relative to space. For a uniformly conducting body, the charging equation is written as

$$\sum J(\Phi_w) = J_e + J_{ea} - (J_i + J_{se} + J_{si} + J_{bse} + J_{ph}) = 0 \quad (1)$$

where J_i and J_e are the ion and electron current densities from the cold ambient plasma, respectively, J_{ea} is the auroral electron current density, J_{se} and J_{si} are the secondary-electron current emissions due to incident electrons and ions, respectively, J_{bse} is the backscattered-electron current, and J_{ph} is the photoelectron current.

To determine the free-flyer potential Φ_w, one needs to know all of the currents collected by the free flyer as a function of Φ_w. For our problem, all electron currents can be calculated analytically or semianalytically. However, because of the complex wake structure, the ion current collected by a free flyer in the wake, J_i, can only be determined numerically. Here we shall first analyze the charging potential Φ_w as a function of J_i.

To a good approximation, the ambient plasma may be modeled as a cold Maxwellian distribution. Since $v_{te} \gg V_0$, the incident electron current from the ambient plasma is simply the random thermal flux. To the order of V_0/v_{te}, the electron density in the vicinity of a negatively charged body is given by the Maxwell-Boltzmann distribution[15]: $n_e \simeq n_0 \exp(e\Phi/KT_e)$. Hence, the incident ambient electron current is given by:

$$J_e(\Phi_w) \simeq \frac{1}{4} e n_e \langle v_{te} \rangle = n_0 \sqrt{\frac{KT_e}{2\pi m_e}} \exp\left(\frac{e\Phi_w}{KT_e}\right) = J_{e0} \exp\left(\frac{e\Phi_w}{KT_e}\right) \quad (2)$$

The best data available on auroral electron energy distributions are the DMSP F6 and F7 data presented in Refs. 3 and 4. It was shown that the high-energy tail of the auroral electron population can be fitted by a Maxwellian distribution. Since this paper concerns the highly negative charging situation and only the high-energy electrons make a significant contribution to the charging potential, it is adequate to model the auroral electrons also as a Maxwellian distribution. Hence, the local auroral electron density is $n_{ea} \simeq n_{ea0} \exp(e\Phi/KT_{ea})$, and the incident auroral electron current is

$$J_{ea}(\Phi_w) \simeq \frac{1}{4} e n_{ea} \langle v_{tea} \rangle = e n_{ea0} \sqrt{\frac{KT_{ea}}{2\pi m_e}} \exp\left(\frac{e\Phi_w}{KT_{ea}}\right) = J_{ea0} \exp\left(\frac{e\Phi_w}{KT_{ea}}\right) \quad (3)$$

The calculations of the photoelectron (J_{ph}), backscattered-electron (J_{bse}), and secondary-electron (J_{se} and J_{si}) currents have been discussed in detail in previous spacecraft charging studies (for example, see Refs. 22–25). Since our electron-current model is the same as that used in these references, their calculations of J_{se} and J_{bse} can be directly applied. In this paper, J_{se}, J_{bse}, and J_{ph} are calculated using the parametrized expressions given in Refs. 25 and 26. For J_{se} and J_{bse}, the secondary-electron yield and backscatter parameters as functions of incident electron energy are taken for that of an aluminum surface [see Eqs. (12) and (21) in Ref. 25]. J_{si} cannot be calculated in a semianalytical way, because the incident ion current J_i will be estimated from particle simulation results.

For simplicity, J_{si} (which reduces charging) will be neglected. This assumption may cause the charging potential to shift somewhat towards the negative end. However, since J_{si} is at most[22,25] of the same order of magnitude as J_i, and within the wake J_i is very small compared to other currents, this shift will not be significant.

In Fig. 2 we show the root of the charging equation vs $\hat{J}_i$ under three different conditions:

1) Nightside, auroral electron: the spacecraft is in the nightside region with auroral electrons.

2) Dayside, auroral electron: the spacecraft is in the sunlit region with auroral electrons.

3) Nightside, no auroral electron: the spacecraft is in the nightside region without auroral electrons.

Under the sunlit or no-auroral-electron condition, the root of the charging equation (1) is about the same order of magnitude as the ambient electron temperature T_e (because of the photoelectron emissions and the absence of high-energy electron flux). At such a low voltage, multibody interaction is usually not an issue of concern, because the electric disturbance will be shielded out in the immediate vicinity of the spacecraft. However, under the nightside, auroral-electron situation, Fig. 2 shows that the charging potential is a very sensitive function of J_i and there exists a high-voltage charging state.

For the plasma parameters considered here, we find Φ_w jumps from $-\hat{\Phi}_w \sim 1$ to $-\hat{\Phi}_w \gtrsim 10^4$ when the ion current collection is reduced to $\hat{J}_i < 10^2$. The nightside, auroral-electron situation is a necessary condition for severe wake charging.

Ion-Current Calculation: Computer Particle Simulation

Next we need to determine the ion-current collection by the free flyer, which requires a self-consistent calculation of the ion trajectories and the electric field in the wake. This problem is solved by using a hybrid particle-in-cell code in which the electrons are treated as a Boltzmann fluid and the ions are treated as particles. This code is an extension of the code used in our previous spacecraft-plasma interaction studies.[18,27]

We shall consider a two-dimensional problem in a moving frame fixed with spacecraft. In the vicinity of negatively biased bodies, the electric field (to the order of V_0/v_{te}) is given by

$$\nabla^2\Phi \simeq -4\pi e[n_i - n_0\exp(e\Phi/KT_e) - n_{ea0}\exp(e\Phi/KT_{ea})] \quad (4)$$

and the boundary conditions at the object-plasma interface. The ion density n_i is determined from the ion trajectories. In the code, a drifting Maxwellian ion beam with a Mach number $M_0 = V_0/C_s = 8$ and a temperature $T_i = 0.5T_e$ is injected from the upstream boundary. The geomagnetic field effect on the ion motion is neglected, because the ion Larmor radius $R_{ci} = V_0/\Omega_i \simeq 36$ m is large compared to the dimensions of a typical satellite. The ion trajectories are calculated by following the motion of test particles from

$$m_i\frac{\mathrm{d}\boldsymbol{v}}{\mathrm{d}t} = -e\nabla\Phi \quad (5)$$

The ion current to the free flyer is then determined by counting the collected test particles.

When a polar spacecraft encounters auroral electrons, the charging time is often much less than the minimum time the spacecraft spends inside the auroral current sheet. Hence, we are interested only in the steady-state charging potential. The steady-state free-flyer potential is calculated from the current balance equation (1) with the numerically determined J_i and analytically evaluated electron currents.

Both the plate and the free flyer are assumed to be prefect absorbers. The dimensions of the system are as follows: the front plate is taken to be a zero-thickness plate with a length of $L_p = 80\lambda_D$ (half plate length $R = 40\lambda_D$), and the free flyer to be an $8\lambda_D \times 8\lambda_D$ box. The flow direction is taken to be the x direction.

Since the number of test particles being traced in the code is much less then the real number of ions, there will be no test particles at certain cells in the deep wake location. This results in a zero ion density (and thus a zero ion current) at the grid points around these cells. While the truncation to $n_i = 0$ does not affect the wake structure (n_i is very small at these points), it may affect the charging calculation for a free flyer in the deep wake. Hence we set a lower-bound background n_i and J_i at these grid points. The lower-bound values of n_i and J_i are the analytical solution of the quasineutral wake presented in Ref. 18.

III. Charging in the Wake Behind a Floating-Potential Plate

Wake and the Severe-Charging Zone

We first consider charging in the wake of a conducting plate whose potential is left floating. Since the ram ion current collected by the front plate is $\hat{J}_i \simeq 8$, from Fig. 2, this ram ion current is large enough to keep the front plate always stay at a near-zero floating potential ($-\hat{\Phi}_p \simeq 0$). For a near-zero-potential plate, the wake structure is a superposition of the two expansion fans generated by the plate edge.[18] (The presence of auroral electrons will not change this wake structure because of their low density.) Each family of expansion waves is described by[18]

$$\ln\frac{n_i}{n_0} \simeq \ln\frac{n_e}{n_0} = \frac{e\Phi}{KT_e} = -\sqrt{M_0^2 - 1}(\theta_0 \pm \theta) - \frac{1}{2}(\theta_0 \pm \theta)^2 \quad (6)$$

where $\theta_0 = \sin^{-1}(M_0^{-1})$ is the Mach angle ($\theta_0 \simeq 7.1$ deg for $M_0 = 8$) and θ is the angle between the expansion characteristic line and the ambient flow direction. Equation (6) shows that both ion and electron density decrease monotonically towards the wake axis. Hence, the plate leaves behind it a triangular-shaped ion-void wake. The two-dimensional (2D) wake structure obtained by particle simulation is shown in Fig. 3. The center of the plate is located at $\hat{x}_p = 30$, $\hat{y}_p = 90$.

It is instructive to compare the magnitudes of the ambient ion and electron flux densities with that of the auroral electron flux density in an empty wake. In Fig. 4a, we plot a magnitude comparison for $\hat{J}_i$, $\hat{J}_e$, and $\hat{J}_{ea}$ at cross section $\hat{x} = 50$ ($\hat{x} - \hat{x}_p = 20$ behind the plate). In an empty wake, the auroral flux of electrons stays almost constant ($\hat{J}_{ea} \simeq 7.64 \times 10^{-2}$) because of their high energy. $\hat{J}_{ea}$ exceeds both the ambient ion and electron fluxes in the deep wake. One can divide an empty wake into three zones based on the relative magnitudes of $\hat{J}_i$, $\hat{J}_e$, and $\hat{J}_{ea}$:

Zone I: $1 \times 10^{-2} < \hat{J}_i < \hat{J}_{ea} \simeq 7.64 \times 10^{-2}$ and $\hat{J}_{ea} < \hat{J}_e$.

Zone II: $\hat{J}_i < 1 \times 10^{-2}$ and $7.64 \times 10^{-2} \simeq \hat{J}_{ea} < \hat{J}_e$.

Zone III: $\hat{J}_i < 1 \times 10^{-2}$ and $\hat{J}_e < \hat{J}_{ea} \simeq 7.64 \times 10^{-2}$.

The division at 1×10^{-2} for J_i approximately corresponds to the turning point of curve 1 in Fig. 2, where $-\hat{\Phi}_w$ starts to jump to the high-level charging state. The three zones are shown in Fig. 4b.

Figure 4b may be used as a first-order charging map to identify the region within which severe wake charging may occur. For instance, in zone I and the outer region of zone II, since $J_e \gg J_{ea}$, the order of magnitude of the charging potential is approximately $\hat{\Phi}_w \sim \ln(J_i/J_{e0})$ ($\hat{J}_{e0}\exp(\hat{\Phi}_w) - \hat{J}_i \simeq 0$). Since $\hat{J}_i$ is also not too much smaller than $\hat{J}_e$, the currents will only allow a charging po-

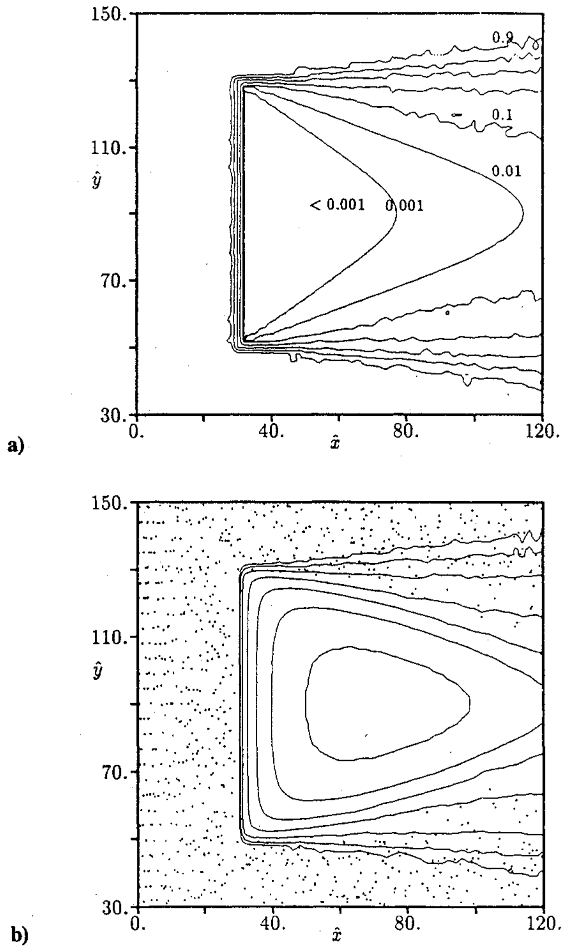

Fig. 3 Empty wake behind a floating plate ($\hat{\Phi}_P \simeq 0$). a) Ion-density contours. Contour levels are at n_i/n_0 = 0.9, 0.7, 0.5, 0.3, 0.1, 0.01, and 0.001. The n_i/n_0 = 0.01 and 0.001 contours come from the analytical quasineutral wake solution,[18] which is used as a lower-bound background for n_i in the simulation. b) Potential contours and ion positions (dots). Contour levels are at $\hat{\Phi}_w$ = −0.25, −0.5, −1, −2, −3, −4, and −5.

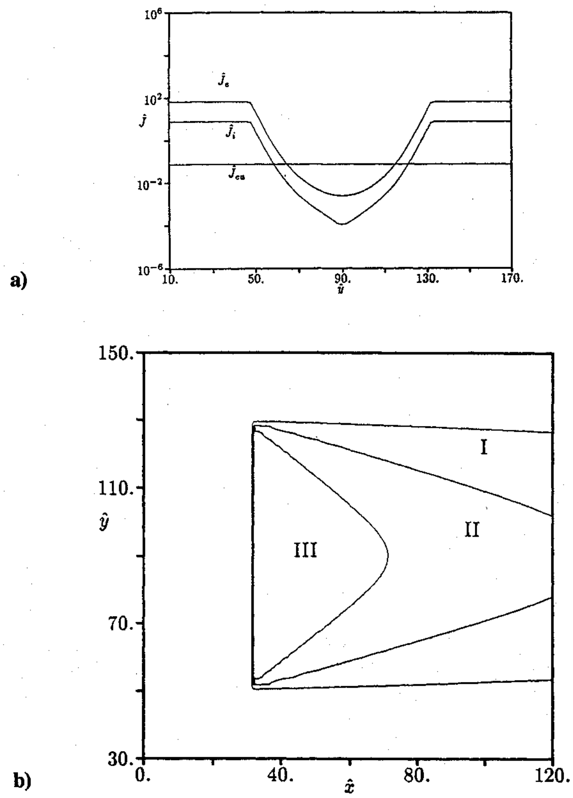

Fig. 4 Comparison of ambient current-density magnitudes in the empty wake behind a floating plate ($\Phi_p \simeq 0$, no free flyer). a) Current-density magnitudes at a cross section $(x_w - x_p)/R = 0.5$ behind the plate. b) Zone I, zone II, and zone III.

tential of the same order of magnitude as the low ambient electron temperature T_e. On the other hand, within zone III, the ion current is reduced to $\hat{J}_i < 10^{-2}$ and the auroral electrons dominate the electron current. From the curve 1 in Fig. 2, we find the currents in zone III allow Φ_w to achieve the high-charging state. Since all the necessary severe charging conditions are satisfied within zone III, this zone can be called the severe-charging zone. Under the nightside, auroral-electron condition, a free flyer within zone III is susceptible to high-voltage charging. The region of zone III can be determined analytically from

$$\exp\left[\frac{e\Phi(x,y)}{KT_e}\left(1-\frac{T_e}{T_{ea}}\right)\right] \le \frac{n_{ea0}}{n_0}\sqrt{\frac{T_{ea}}{T_e}} \tag{7}$$

where Φ is given by Eq. (6).

Charging in the Wake of a Floating Plate

We now put a free flyer in the wake. A typical simulation result is shown in Fig. 5. The ambient plasma flow is in the x direction. The center of the free flyer is at $(x_w - x_p)/R = 0.5$ behind the plate on the central axis in the wake ($\hat{x}_w = 50$, $\hat{y}_w = 90$). Figure 5a shows the situation when no auroral electrons are involved. The free-flyer floating potential in Fig. 5a is $\hat{\Phi}_w \simeq -15.6$. In the absence of auroral electrons, a free flyer can be charged to no more than a few volts negative because the electron temperature $T_e \sim 0.1$ eV. In this situation, the presence of the free flyer does not affect the overall wake structure.

Figure 5b shows the result for the nightside, auroral-electron condition. The free flyer is at the same location. Because of the auroral-electron current, the free flyer is charged to about $\hat{\Phi}_w \simeq -1.9 \times 10^3$. The sheath surrounding the free flyer now grows outside the wake dimension and dominates the original wake structure. The electric field of the free flyer attracts the ambient ions into the wake, overcomes their angular momentum barrier, and collects enough of them to achieve total current balance.

In Fig. 6, we show the free-flyer charging potential at several locations in the wake. Figure 6a shows the charging potential along the central axis (line 1) and an off axis (line 2) in the

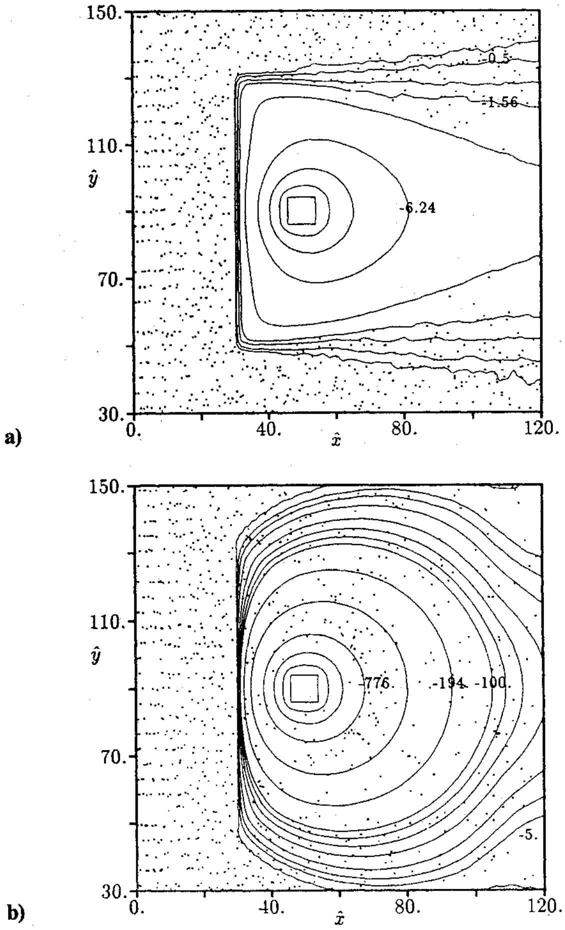

Fig. 5 Charging in the wake of a floating plate: potential contours and ion positions. The center of the free flyer is on axis at $x/R = 0.5$ downstream. a) No-auroral-electron condition. $\hat{\Phi}_w \simeq -15.6$. Contour levels at $\hat{\Phi} = \hat{\Phi}_w, 0.8\hat{\Phi}_w, 0.6\hat{\Phi}_w, 0.4\hat{\Phi}_w, 0.2\hat{\Phi}_w, 0.1\hat{\Phi}_w, -1, -0.5$, and -0.25. b) Nightside, auroral-electron condition. $\hat{\Phi}_w \simeq -1940$. Contour levels at $\hat{\Phi} = \hat{\Phi}_w, 0.8\hat{\Phi}_w, 0.6\hat{\Phi}_w, 0.4\hat{\Phi}_w, 0.2\hat{\Phi}_w, 0.1\hat{\Phi}_w, -100, -80, -60, -40, -20, -10, -5$, and -1.

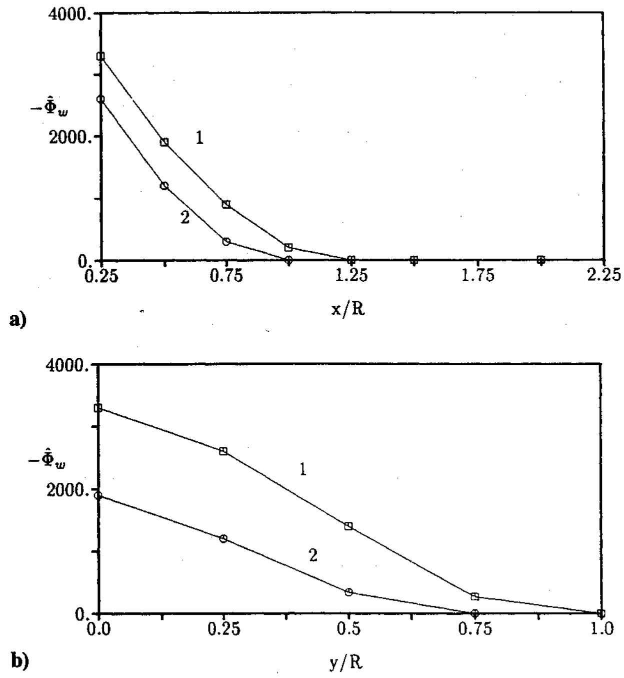

Fig. 6 Free-flyer charging potential. a) Potential along the flow direction. Curve 1: central wake axis; curve 2: off axis with $(y_w - y_p)/R = 0.25$. b) Potential along wake cross sections downstream from the plate. Curve 1: $(x_w - x_p)/R = 0.25$; curve 2: $(x_w - x_p)/R = 0.5$.

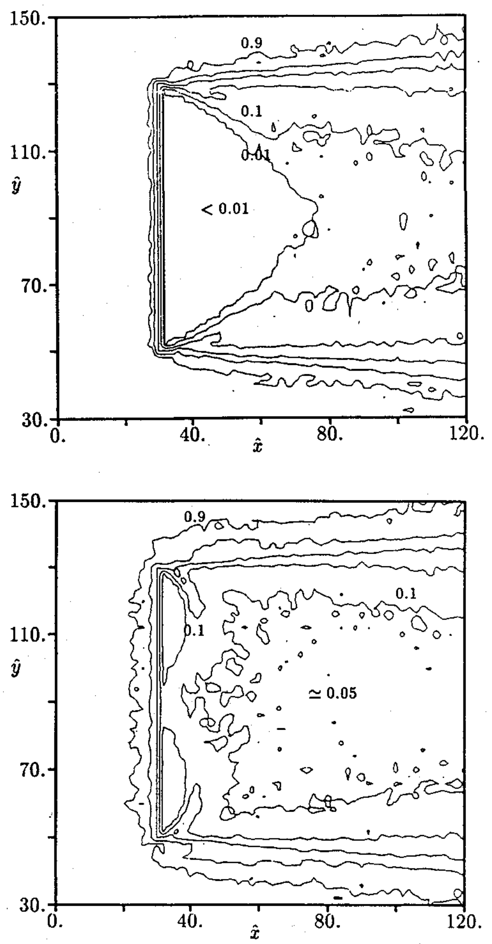

Fig. 7 The empty wake behind a biased plate: ion-density contours. a) $\hat{\Phi}_p = -20$. Contour levels at $n_i/n_0 = 0.9, 0.7, 0.5, 0.3, 0.1$, and 0.01. b) $\hat{\Phi}_p = -80$. Contour levels at $n_i/n_0 = 0.9, 0.7, 0.5, 0.3$, and 0.1.

flow direction. The distance of the off axis from the central axis is $(y_w - y_p)/R = 0.25$. Figure 6b shows the charging potential along two wake cross sections parallel to the plate. The first cross section is at $(x_w - x_p)/R = 0.25$ from the plate (line 1), and the second cross section is at $(x_w - x_p)/R = 0.5$ (line 2). If the flyer is far away from the plate in the flow direction or far away from the central wake axis, its charging potential is low, because the local ambient ion current is sufficient to balance the electron current. However, as the flyer approaches the front plate within the deep wake, its charging potential starts to increase significantly, because the auroral electrons dominate the electron current and there is insufficient ion current to balance the electron current. Not surprisingly, the locations where a free flyer has a high negative potential are within the severe-charging zone (zone III in Fig. 4b).

IV. Charging in the Wake of a Biased Plate

There are situations in which the front plate may acquire a large voltage. For instance, the operation of a high-voltage power system can drive part of a large structure to a very negative potential. Recently, Wang and Hastings[18] studied the wake structures for typical large high-voltage space platforms and found that a negatively biased plate generates a space-charge wake structure. Depending on the plate dimension and plate voltage, significant ion backflow can occur in a space-charge wake. (See Ref. 18 for detailed discussions on the plasma wake behind a biased plate.)

In this section, we study the effects of the front-plate voltage Φ_p on wake charging. We shall consider two front-plate voltages: $\hat{\Phi}_p = -20$ and $\hat{\Phi}_p = -80$. Figure 7 shows the empty-wake structures for these two biased plates. The value of Φ_p is chosen so that the ratio of sheath thickness to plate dimension,[18] $\zeta \simeq d_{sh}/L_p \simeq 0.8|\hat{\Phi}_p|^{\frac{3}{4}}/(\hat{L}_p\sqrt{M_0})$, is in the same range of that for practical space platforms. In most practical situations of interest to us, the dimension and voltage of a space platform put its sheath ratio in the range of $\zeta \sim 10^{-2}$ to 10^{-1} (see Ref. 18). For $\hat{\Phi}_p = -20$ and $\hat{L}_p = 80$, we have $\zeta \sim 0.033$, which is about the same as that for a 10-m plate biased at −30 V. For $\hat{\Phi}_p = -80$ and $\hat{L}_p = 80$, we have $\zeta \simeq 0.095$, which is about the same as that for a 10-m plate biased at −125 V. Therefore, the $\hat{\Phi}_p = -20$ case represents a "low-voltage" biased plate and the $\hat{\Phi}_p = -80$ case represents a "high-voltage" biased plate.

In Fig. 8, we compare the free-flyer charging in the wake of a biased plate with that for a floating plate. The charging potentials are all calculated for the nightside, auroral-electron situation. The location of the free flyer is along the central axis in the wake. When the front plate is biased at $\hat{\Phi}_p = -20$, the plate voltage pulls the ambient ions into the wake, resulting in a much shorter ion-void region than that in a quasineutral wake (Fig. 7a). Hence, the charging level at locations $(x_w - x_p)/R > 0.75$ is lower than that in the floating-plate case. However, the charging level at locations $(x_w - x_p)/R \leq 0.75$ is still the same as that in the $\hat{\Phi}_p \simeq 0$ situation, because an ion-void region still exists in the near wake. Hence, for this "low-voltage" case, all discussions of Sec. 3 on wake charging still apply to the near-wake region.

When the front plate is biased at $\hat{\Phi}_p = -80$, the high plate voltage creates an ion backflow in the wake, and the ion-void triangle is now reduced to two ion-void "holes" (Fig. 7b). There are sufficient ions everywhere along the central axis in the wake to balance the electrons collected by the free flyer. Therefore, we find the free-flyer charging potential remains at $\Phi_w \sim T_e$. The slight decrease of $|\Phi_w|$ at $(x_w - x_p)/R = 0.25$ is caused by local ion-density enhancement around that location.

Figure 9 shows the electric potential and ion positions for the $\hat{\Phi}_p = -80$ case. Again, the location of the free-flyer center is taken to be $(x_w - x_p)/R = 0.5$, $y_w = y_p$. The free flyer is charged to

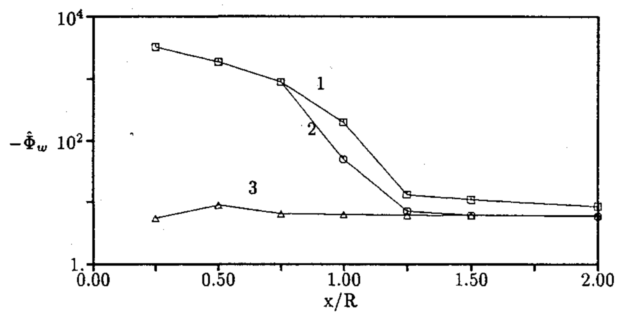

Fig. 8 Comparison of $\hat{\Phi}_w$ in the wake of biased plates with that of the floating plate. The free-flyer location is along the central wake axis. Curve 1: floating plate ($-\hat{\Phi}_p \simeq 0$); curve 2: biased plate with $\hat{\Phi}_p = -20$; curve 3: biased plate with $\hat{\Phi}_p = -80$.

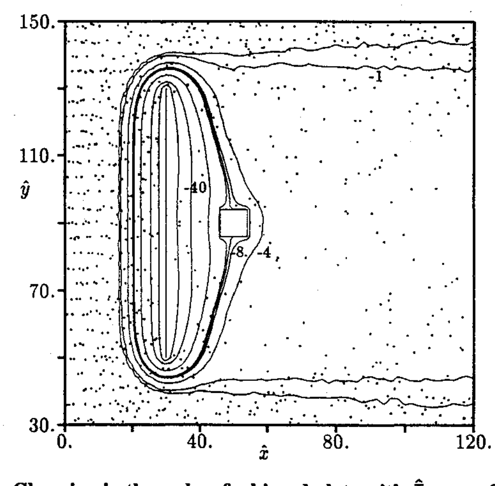

Fig. 9 Charging in the wake of a biased plate with $\hat{\Phi}_p = -80$, $\hat{\Phi}_w \simeq -9$: potential-contour map and ion positions. The center of the free flyer is on axis, $x/R = 0.5$ downstream. Contour levels at $\hat{\Phi} = -80, -60, -40, -20, -10, -9, -8, -4, -1$, and −0.5.

$\hat{\Phi}_w \simeq -9$. It is interesting to point out that although severe charging does not occur on the free flyer in this situation, a large potential difference still exists between the free flyer and the plate, because the front plate now has a high biasing potential. Hence, MPI will still occur within the sheath region of the front plate.

V. Conclusions

We have studied interactions between a large plate and a small free flyer in its wake. The wake structure, the ion trajectories, and the ion current collection and charging potential of the free flyer are found self-consistently, using computer particle simulations coupled with charging-potential calculations. For a floating plate, a severe-charging zone for the free flyer exists in the near wake under the nightside, auroral-electron condition. Hence, MPI occurs as a result of this high-voltage wake charging. If the plate has a low biasing voltage, the interaction in the near wake is similar to that in the floating-plate case. But in the midwake, the free flyer's charging potential is reduced because of the smaller size of the ion-void region. In the wake of a highly biased plate, the free-flyer potential remains at $\Phi_w \sim T_e$ due to the ion backflow caused by the plate potential. When the free flyer enters the sheath region of the plate, MPI occurs due to the potential difference between the free flyer and the high-voltage plate.

Wake charging and the resulting multibody interactions may have significant implications for astronauts on extravehicular activities and docking operations. For instance, an important risk factor for EVA is the charging level during geomagnetically active periods. Based on the charging calculations in this paper, we conclude that the severe charging zone of the shadowing vehicle should always be avoided. However, astronaut charging should not be a factor of concern for EVA outside the severe charging zone. (Under sunlit or no-auroral-electron condition, the entire wake region is safe for EVA.) Another typical concern that mission planners have is whether electrostatic discharge might occur during a docking operation. In the case of docking in the wake under nightside, auroral-electron conditions, we find that a large potential difference will always exist between the main vehicle and the docking vehicle, no matter whether the main vehicle floats at a near-zero potential or is biased to a very negative potential. Hence, arc discharges may be a real concern. In contrast, docking on the ram side of a near-zero potential structure reduces the potential difference, and thus is a relatively safe configuration. In this paper, we only considered a simple 2D steady-state two-body problem. In the future, the analysis will be extended to three dimensions and more complex systems. Transient wake charging and docking-induced ESD problems will also be studied.

Acknowledgments

This work was carried out at the Jet Propulsion Laboratory under a contract with NASA. Computational support was provided by the JPL Supercomputing Project, which is sponsored by JPL and the NASA Office of Space Science and Applications. The authors would like to acknowledge many useful discussions with R. Biasca and M. Mandell and computational assistences from B. Ruff.

References

[1]Ferguson, D., Snyder, D., and Carruth, M. (eds.), "Evaluation of Impacts of Space Station Freedom Grounding Configurations," NASA TM 103717, May 1990.

[2]Leung, P., "Multibody Interactions in Plasmas," Jet Propulsion Lab., JPL D-6752, Sept. 1989.

[3]Gussenhoven, M. S., Hardy, D. A., Rich, F., Burke, W. J., and Yeh, H.-C., "High-Level Spacecraft Charging in the Low-Altitude Polar Auroral Environment," *Journal of Geophysical Research*, Vol. 90, No. 11, 1985, pp. 11009–11023.

[4]Yen, H.-C., and Gussenhoven, M. S., "The Statistical Electron Environment for Defense Meteorological Satellite Program Eclipse Charging," *Journal of Geophysical Research*, Vol. 92, No. 7, 1987, pp. 7705–7715.

[5]Katz, I., Parks, D. E., Cooke, D. L., Mandell, M. J., and Rubin, A. J., "Polar Orbit Electrostatic Charging of Objects in Shuttle Wake," *Spacecraft Environmental Interactions Technology 1983*, NASA Lewis Research Center, 1985, pp. 229–234.

[6]Katz, I., Mandell, M. J., Jongeward, G. A., Lilley, J. R., Hall, W. N., and Rubin, A. G., "Astronaut Charging in the Wake of a Polar Orbiting Shuttle," AIAA Paper 85-7035, Nov. 1985.

[7]Laframboise, J. G., and Luo, J., "High-Voltage Polar-Orbit and Beam-Induced Charging of a Dielectric Spacecraft: A Wake-Induced Barrier Effect Mechanism," *Journal of Geophysical Research*, Vol. 94, No. 7, 1989, pp. 9033–9048.

[8]Troim, J., and Maehlum, B. N., "Laboratory Simulation Studies on Charging of Spacecraft," *Physics of Charged Bodies in Space Plasmas*, edited by M. Dobrowolny and E. Sindoni, Varenna, Italy, 1991, pp. 305–313.

[9]Enloe, C. L., Cooke, D. L., Meassick, S., Chan, C., and Tautz, M. F., "Ion Collection in a Spacecraft Wake: Laboratory Simulations," *Journal of Geophysical Research*, Vol. 98, No. 8, 1993, pp. 13635–13644.

[10]Fournier, G., and Pigache, D., "Wakes in Collisionless Plasma," *Physics of Fluids*, Vol. 18, 1975, pp. 1443–1453.

[11]Stone, N. H., "The Plasma Wake of Mesosonic Conducting Bodies. Part 1. An Experimental Parametric Study of Ion Focusing by the Plasma Sheath," *Journal of Plasma Physics*, Vol. 25, 1981, pp. 351–371.

[12]Merlino, R. L., and D'Angelo, N., "The Interaction of a Conducting Object with a Supersonic Plasma Flow: Ion Deflection Near a Negatively Charged Obstacle," *Journal of Plasma Physics*, Vol. 37, 1987, pp. 185–198.

[13]Meassick, S., Chan, C., Qian, Y., Sroda, T., Azar, T., and Allen, R. C., "Temporal Study of Wake Formation behind a Conducting Body," *Journal of Geophysical Research*, Vol. 96, No. A8, 1991, pp. 13985–13995.

[14]Latham, P. M., Bond, R. A., Pearce, A. J., and Martin, A. R., "Laboratory Simulations of Spacecraft/Plasma Wake Phenomena and Comparison with Computational Predictions," *Physics of Charged Bodies in Space Plasmas*, edited by M. Dobrowolny and E. Sindoni, Varenna, Italy, 1991, pp. 37–62.

[15]Liu, V. C., "Ionospheric Aerodynamics of Satellites and Diagnostic Probes," *Space Science Review*, Vol. 9, 1969, pp. 423–490.

[16]Gurevich, A. V., Pitaevskii, L. P., and Smirnova, V. V., "Ionospheric Aerodynamics," *Space Science Reviews*, Vol. 9, 1969, pp. 805–871.

[17]Martin, A. R., "Numerical Solutions to the Problem of Charged Particle Flow around an Ionospheric Spacecraft," *Journal of Plasma Physics*, Vol. 22, 1974, pp. 121–141.

[18]Wang, J., and Hastings, D. E., "Ionospheric Plasma Flow over Large High-Voltage Space Platforms. II: The Formation and Structure of Plasma Wake," *Physics of Fluids B*, Vol. 4, No. 6, 1992, pp. 1615–1629.

[19]Samir, U., Stone, N. H., and Wright, K. H., "On Plasma Disturbances Caused by the Motion of the Space Shuttle and Small Satellites: A Comparison on In Situ Observations," *Journal of Geophysical Research*, Vol. 91, No. A1, 1986, pp. 277–285.

[20]Raitt, W. J., Eccles, J. V., Thompson, D. C., Banks, P. M., Williamson, P. R., and Bush, R. I., "Plasma Parameters in the Near Wake of the Space Shuttle," *Geophysical Research Letters*, Vol. 14, No. 4, 1987, pp. 359–362.

[21]Murphy, G. B., Reasoner, D. L., Tribble, A., D'Angelo, N., Pickett, J., and Kurth, W. S., "The Plasma Wake of the Space Shuttle Orbiter," *Journal of Geophysical Research*, Vol. 94, No. 6, 1989, pp. 6866–6872.

[22]Garrett, H. B., "The Charging of Spacecraft Surfaces," *Reviews of Geophysics and Space Physics*, Vol. 19, No. 4, 1981, pp. 577–616.

[23]Whipple, E. C., "Potentials of Surfaces in Space," *Reports on Progress in Physics*, 44, 1981, pp. 1199–1250.

[24]Katz, I., Mandell, M. J., Jongeward, G., and Gussenhoven, M. S., "The Importance of Accurate Secondary Electron Yields in Modeling Spacecraft Charging," *Journal of Geophysical Research*, Vol. 91, No. 12, 1986, pp. 13739–13744.

[25]Tsipouras, P., and Garrett, H. B., "Spacecraft Charging Model—Two Maxwellian Approximation," Air Force Geophysics Lab., AFGL-TR-79-0153, 1979.

[26]Garrett, H. B., "Spacecraft Potential Calculations—A Model," Air Force Geophysics Lab., AFGL-TR-78-0116, 1978.

[27]Wang, J., and Hastings, D. E., "Ionospheric Plasma Flow over Large High-Voltage Space Platforms. I: Ion-Plasma-Time Scale Interactions of a Plate at Zero Angle of Attack," *Physics of Fluids B*, Vol. 4, No. 6, 1992, pp. 1597–1614.